Clinical Radiology 78 (2023) e319–e327

Contents lists available at ScienceDirect

Clinical Radiology

journal homepage: www.clinicalradiologyonline.net

Lung parenchyma and structure visualisation in paediatric chest MRI: a comparison of different short and ultra-short echo time protocols

D. Papp [a,*], B. Elders [a,b], P.A. Wielopolski [a], G. Kotek [a], M. Vogel [c], H.A.W.M. Tiddens [a,b], P. Ciet [a,b], J.A. Hernandez-Tamames [a]

[a] *Department of Radiology and Nuclear Medicine, Erasmus Medical Centre, Rotterdam, the Netherlands*
[b] *Department of Paediatric Pulmonology and Allergology, Erasmus Medical Centre—Sophia Children's Hospital, Rotterdam, the Netherlands*
[c] *General Electric Healthcare, Waukesha, WI, USA*

ARTICLE INFORMATION

Article history:
Received 30 September 2022
Accepted 23 December 2022

AIM: To evaluate image quality acquired at lung imaging using magnetic resonance imaging (MRI) sequences using short and ultra-short (UTE) echo times (TEs) with different acquisition strategies (breath-hold, prospective, and retrospective gating) in paediatric patients and in healthy volunteers.

MATERIALS AND METHODS: End-inspiratory and end-expiratory three-dimensional (3D) spoiled gradient (SPGR3D) and 3D zero echo-time (ZTE3D), and 3D UTE free-breathing (UTE3D), prospective projection navigated radial ZTE3D (ZTE3D vnav), and four-dimensional ZTE (ZTE4D) were performed using a 1.5 T MRI system. For quantitative assessment, the contrast-to-noise ratio (CNR) and signal-to-noise ratio (SNR) values were calculated. To evaluate image quality, qualitative scoring was undertaken on all sequences to evaluate depiction of intrapulmonary vessels, fissures, bronchi, imaging noise, artefacts, and overall acceptability.

RESULTS: Eight cystic fibrosis (CF) patients (median age 14 years, range 13–17 years), seven children with history of prematurity with or without bronchopulmonary dysplasia (BPD; median 10 years, range 10–11 years), and 10 healthy volunteers (median 32 years, range 20–52 years) were included in the study. ZTE3D vnav provided the most reliable output in terms of image quality, although scan time was highly dependent on navigator triggering efficiency and respiratory pattern.

CONCLUSIONS: Best image quality was achieved with prospective ZTE3D and UTE3D readouts both in children and volunteers. The current implementation of retrospective ZTE3D readout (ZTE4D) did not provide diagnostic image quality but rather introduced artefacts over the entire imaging volume mimicking lung pathology.

* Guarantor and correspondent: D. Papp, Department of Radiology and Nuclear medicine, Erasmus Medical Centre, Rotterdam, the Netherlands.
E-mail address: d.papp@erasmusmc.nl (D. Papp).

https://doi.org/10.1016/j.crad.2022.12.020

Introduction

Lung magnetic resonance imaging (MRI) with good image quality and high spatial resolution has been a long-desired goal, especially in the paediatric population.[1] To date, computed tomography (CT) still prevails as the main imaging tool for the paediatric lung, because it is fast, simple to execute, and provides diagnostic image quality at any age; however, repeated use of CT in children is limited because of the possible harm from ionising radiation.[2,3] Conversely, MRI, as an ionising radiation-free technique, offers superior inherent soft-tissue contrast and has therefore the potential for robust structure and function assessment in a single examination.[4]

Obtaining high-quality MRI images of the lung has been cumbersome as compared to other anatomical regions[1,5] due to the inherent properties of lung tissue, the surrounding magnetic environment, and breathing motion during MRI signal acquisition.[6] Lung parenchyma has low proton density, hence the signal received is quite low.[7] Conventional gradient echo-based pulse sequences with echo times in the range of milliseconds have limited effectiveness to detect the lung signal, which has a short T2*. Two-dimensional ultrashort echo time (UTE) MRI, first proposed by Bergin *et al.*,[8] could attain the necessary short echo times (nearly zero) in order to appreciate parenchymal signal and structure at higher spatial resolution.[9–14] UTE uses radial k-space sampling in order to sample the rapidly decaying signal right after the radiofrequency (RF) excitation and therefore can counteract the signal loss from transverse relaxation time (T2* decay). Another radial encoding scheme that has recently emerged with zero echo time (ZTE) encoding showed promising results for lung imaging.[28] In this technique, the readout gradients are turned on prior to the RF excitation so that encoding can start simultaneously upon signal excitation resulting in a nearly ZTE. ZTE has the additional benefit of being nearly silent, therefore ideal for neonatal and paediatric imaging.

For paediatric lung MRI, image quality also strongly depends on patient compliance.[5] Short breath-hold (BH) acquisitions can be successfully performed in children from 6 years and older, reducing motion artefacts from respiratory movements. Unfortunately, non-cooperative children and younger ones require free-breathing gated (prospective or retrospective) or ungated strategies.[15–27] Therefore, recent implementations of retrospectively gated UTE3D and ZTE3D sequences show promising results in young children.[28–33] To the authors' knowledge, only very few studies have been conducted comparing conventional and novel short TE sequences for lung imaging.[29–31]

The aim of the present study was to evaluate the performance of short and UTE MRI sequences with different strategies (breath-hold, prospective, and retrospective gating) in paediatric patients and in healthy volunteers for lung imaging and determine which sequence is the most suitable for parenchymal signal detection in paediatric imaging.

Materials and methods

Patients and volunteers

The study was approved by the local Institutional Review Board (MEC2018-134, MEC2018-002). Written informed consent was obtained from all participants or parents and legal guardians before the MRI examinations. From March 2019 to May 2020, patients with either cystic fibrosis (CF) or prematurely born patients with and without bronchopulmonary dysplasia (BPD) underwent chest MRI. Moreover, healthy adult male volunteers were recruited in this study to make standardised comparisons between the different sequence possibilities and scanning scenarios.

Lung MRI

MRI was performed at 1.5 T (Signa Artist, GE Healthcare, USA) using a body coil for excitation and 32-channel signal reception hardware that included a small anterior 16-channels torso array coil and the table embedded spine coil. The MRI protocol included several sequences for lung parenchyma and structure visualisation: Cartesian breath-hold SPGR3D, breath-hold radial ZTE3D (ZTE3D BH), prospective respiratory pneumo-belt gated cones UTE3D, prospective projection navigated radial ZTE3D (ZTE3D vnav) and retrospectively reconstructed multi-phasic radial ZTE3D (ZTE4D) collected during tidal breathing. All sequences were tuned to provide a proton-density weighted (PDW) signal. Table 1 shows the acquisition parameters for each sequence. All scans were reconstructed using 3D gradwarp to compensate for gradient non-linearity at the edges of the field-of-view (FOV) and no surface coil intensity correction was applied. SPGR3D was acquired during a short breath-hold in end-inspiration and end-expiration in all patients and healthy volunteers. For patients, breath-hold manoeuvres were monitored and recorded using an MRI compatible spirometer (Masterscreen Pneumo portable spirometer).[34] The standard pneumo-belt monitoring was used for all participants. Sixteen different respiratory phases were reconstructed retrospectively for ZTE4D based on the recorded pneumo-belt signal. For healthy volunteers, a 20 second ZTE3D BH and an 8 second breath-hold SPGR3D were obtained at five different inspiratory levels from full expiration to full inspiration to have a better comparison with the ZTE4D reconstructed phases. Volunteers were instructed to take one, two, and three small breaths and hold the inspiratory positions until scanning was completed. To compare the ZTE3D BH scans with ZTE4D, three inspiratory levels were chosen that best matched the excursion of the reconstructed phases of the ZTE4D scan. Further details about the prospective pneumo-belt and navigator gating are provided in the Electronic Supplementary Material. For each paediatric patient, at least one ZTE3D vnav and one UTE3D scan had to be performed successfully to be included in the comparative study.

Table 1
Parameters of the used MRI sequences.

Sequence	SPGR3D BH (vol/CF/BPD)	UTE3D[a] (vol/CF/BPD)	ZTE3D vnav (vol/CF/BPD)	ZTE4D (vol)	ZTE3D BH (vol)
Acquisition plane	Sagittal	Axial	Axial	Coronal	Coronal
TR/TE (ms)	1.5/0.6	5.2/0.032	1.1/0	1.4/0	1.25/0
Flip angle (°)	2	3	2	1	2
RF	Selective	Selective	Non-selective	Non-selective	Non-selective
In-plane matrix	120 × 120	228 × 228	200 × 200	150 × 150	150 × 150
K-space trajectory	Cartesian	CONES	Radial	Radial	radial
In-plane FOV	36	34	30	34	34
Rectangular FOV	0.75	—	—	—	—
Actual voxel resolution (mm^3)	3 × 3 × 3	1.5 × 1.5 × 1.5	1.5 × 1.5 × 1.5	2.2 × 2.2 × 2.2	2.2 × 2.2 × 2.2
No. of sections	80–130	230	200	110	110
Section thickness	3	1.5	1.5	2.2	2.2
Receiver bandwidth (kHz)	90	125	62.5	50	62.5
Parallel imaging (ARC)	1.5 × 1.2	None	None	None	None
Number of averages	1	1	2.5	7	1
Number of phases	1	1	1	16	1
No. of spokes per segment	—	120–170	800	64	200
Physiological triggering	Breath-hold	Prospective pneumobelt	Prospective projection navigator	Retrospective pneumobelt	Breath-hold
Scan time (respiratory rate = 20)[b]	5–8 s	4 min 48 s	9 min 50 s	3 min 10 s	20 s

SPGR3D BH, breath-hold three-dimensional spoiled gradient; UTE3D, three-dimensional ultra-short echo time; ZTE3D vnav, three-dimensional prospective projection navigated radial zero echo time; ZTE4D, four-dimensional zero echo time; ZTE3D BH, breath-hold three-dimensional zero echo time; FOV, field-of-view; BDP; bronchopulmonary dysplasia, BH; breath-hold, CF; cystic fibrosis, TE; echo time, TR; repetition time.

[a] In volunteers a ZTE3D acquisition was included.

[b] Scan time was set for a respiratory rate of 20 breaths/min.

Image analysis

All non-axially acquired images were reformatted into the axial plane for comparison, anonymised and randomised for image analysis. Images were reviewed on the Advantage Window Server platform (AWS 2.0).

Quantitative assessment

To compare the ability of the different sequences to perceive lung parenchyma signal and depict normal structures, the signal intensity (SI) of intrathoracic structures was recorded. Contrast-to-noise ratio (CNR) and signal-to-noise ratio (SNR) values were then calculated. Regions of interest (ROIs) were drawn in background air, lung parenchyma, pulmonary artery, and oblique muscles. The ROIs in the lung parenchyma were positioned and sized on the SPGR3D expiration scans so they did not contain major vascular components/fissure; the ROIs were subsequently copied to all the different sequences evaluated per subject and adjusted according to the inspiratory level. The lung parenchyma ROIs were adjusted in case motion-related artefacts were detected. The mean of these six ROIs was then used for the lung parenchyma SNR assessment (see Fig 1). SNR was calculated as the mean SI of the measured structure divided by the standard deviation (STD) of the background outside the thoracic region/body, which was used as reference for the noise.

$$\mathrm{SNR} = \frac{\mathrm{SI}_{\text{lung parenchyma}}}{\mathrm{STD}_{\text{background}}}$$

For ZTE3D vnav, ZTE4D and UTE3D sequences artefactual increase in signal/noise around structures with very short T2* (e.g., coil, coil frame, coil housings) can propagate into the background noise outside the chest, which has to be taken into account. Because of this, SNR calculations were performed with two different background noise STDs: one was taken from an area from background outside the chest (referred to as $\mathrm{SNR}_{\mathrm{out}}$) and the other was taken in the trachea inner lumen ($\mathrm{SNR}_{\mathrm{trachea}}$).

CNRs of the lung parenchyma and pulmonary artery (CNR lung–blood, $\mathrm{CNR}_{\mathrm{LB}}$ indicating visibility of intrapulmonary vessels), the lung parenchyma and oblique muscle (CNR lung–muscle , $\mathrm{CNR}_{\mathrm{LM}}$, indicating visibility of muscles) and the pulmonary artery and oblique muscle (CNR blood–muscle, $\mathrm{CNR}_{\mathrm{BM}}$, to indicate the visibility between artery and muscle) were also measured. The calculations of the CNR values were as follows:

$$\mathrm{CNR}_{\mathrm{LB}} = \frac{\mathrm{mean}(\mathrm{SI\ (pulmonary\ artery)}) - \mathrm{mean\ (SI\ (lung\ parenchyma)})}{\mathrm{STD(background)}}.$$

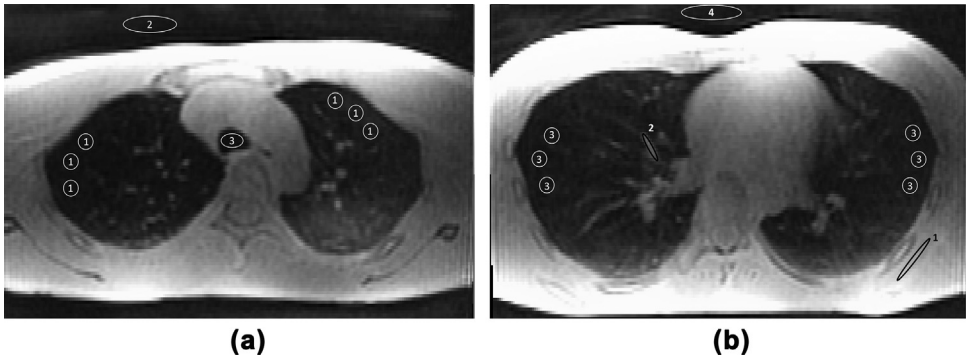

Figure 1 (a) Example of the placement of the ROIs for the SNR calculation in a ZTE4D sequence. Circle 1 provides the mean value for the signal intensity. Standard deviation of ROI 2 was used to calculate SNR_{out} and the SD of ROI 3 was used to calculate $SNR_{trachea}$. (b) Example of the placement of the ROIs for CNR calculation in the same sequence. Mean values were taken from circle 1, oblique muscle; circle 2, pulmonary artery; circle 3, lung parenchyma and the SD of ROI 4 was used to calculate the different CNR values.

$$\mathrm{CNR_{LM}} = \frac{\mathrm{mean(SI\ (oblique\ muscles)) - mean\ (SI\ (lung\ parenchyma))}}{\mathrm{STD(background)}},$$

and the CNR of the pulmonary artery–muscle as

$$\mathrm{CNR_{BM}} = \frac{\mathrm{mean(SI\ (pulmonary\ artery)) - mean\ (SI\ (oblique\ muscles))}}{\mathrm{STD(background)}}.$$

Qualitative assessment

To evaluate the image quality of SPGR3Ds, UTE3D, ZTE3D vnav, ZTE4D, and ZTE3D BH, the depiction of the intrapulmonary vessels, lung fissures, bronchi, imaging noise, artefacts, and overall acceptability were evaluated using a modified version of the scoring system proposed by Bae *et al.*[29] (Table 2) on the expiratory images. Modification consisted of the assessment of bronchi visibility, which was scored by calculation of the amount of lobar, segmental, and sub-segmental bronchi visible in each sequence. All scans were scored in random order by an independent reviewer (B.E.) with 3 years of experience in lung MRI. To test intra- and interobserver reproducibility, the scoring was repeated 3 months after the original measurements, and all scans were also scored by a second reviewer (P.C.) with 10 years of experience in lung MRI.

Statistical analyses

Differences between sequences in SNR and CNR were compared with a paired *t*-test. Image quality was assessed with descriptive statistics. Intra- and interobserver agreement was assessed using the intra-class correlation coefficient and Bland–Altman plots. Statistical tests were performed using IBM SPSS Statistics.

Results

Eight CF patients (age range 13–17 years, median 14 years), seven children with a history of prematurity with or without BPD (age range 10–11 years, median 10 years), and 10 volunteers (age range 20–52 years, median 32 years) were included in the present study.

Table 1 shows examples of scans from a healthy volunteer and figures are available from the Electronic Supplementary Material. Figs 2 and 3 show exemplary scans from CF and BPD patients. SPGR3D expiration and inspiration, UTE3D, ZTE3D vnav were performed on volunteers and patients (n=25), but due to scan time limitations, ZTE4D and ZTE3D breath-hold scans were performed only on volunteers (n=10).

ZTE4D captured the entire respiratory cycle with the number of phases selected; nonetheless, most of the phases around tidal inspiration and well into expiration had reconstruction artefacts with only a very limited number of

Table 2
Qualitative assessment of MRI sequences, adapted and modified from Bae *et al.*[29]

Depiction of the intrapulmonary vessels
1. Unacceptable (invisible peripheral pulmonary vessels)
2. Poor (barely visible peripheral pulmonary vessels)
3. Fair (visible peripheral pulmonary vessels)
4. Good (visible peripheral pulmonary vessels with clear margin)
5. Excellent (visible peripheral pulmonary vessels with clear margin)
Depiction of fissures
1. Unacceptable (invisible interlobar fissure)
2. Fair (blurred lobar fissure)
3. Good (visible interlobar fissure)
Depiction of the bronchus
1. Unacceptable (indistinguishable lobar bronchial walls)
2. Poor (visible lobar bronchial walls with <10 visible segmental bronchial walls)
3. Fair (visible lobar bronchial walls with >10 visible segmental bronchial walls)
4. Good (visible lobar bronchial walls with >10 visible segmental bronchial walls, with few visible sub/segmental bronchial walls)
5. Excellent (visible sub-subsegmental bronchial walls)
Image noise/artefacts (cardiac, respiratory and streaking)
1. Unacceptable
2. Above-average noise/artefacts
3. Average and acceptable
4. Less than average
5. Minimum or nothing
Overall acceptability
1. Unacceptable
2. Suboptimal
3. Satisfactory
4. Above average
5. Superior

phases around the end-expiratory period providing a clean image with adequate sharpness.

Quantitative assessment

The results of the quantitative analyses are shown in Table 3. SNRs were measured on expiratory and inspiratory scans separately, because of the higher lung parenchyma density (lower amount of air) in expiration, which provided higher SNR values. The SNR_{out} had the highest value for SPGR3D in deep expiration, followed by ZTE4D (p=0.4391). SPGR3D in inspiration had lower SNR values than ZTE3D BH inspiration.

CNR_{LB} was significantly higher for SPGR3D in end-inspiration and in end-expiration than for ZTE3D BH in both conditions (all p<0.001). CNR_{LM} was significantly higher in SPRG3D inspiration than expiration (p=0.0085). SPGR3D inspiration had the highest CNR, followed by ZTE3D BH inspiration (p=0.2960). The CNR of blood–muscle was highest on the two inspiratory breath-hold sequences, and significantly lower on UTE3D (UTE3D versus ZTE3D BH: p<0.0001, UTE3D versus SPGR3D: p=0.0003).

Qualitative assessment

Image quality was highest for UTE3D for noise and overall acceptability, and highest for ZTE3D vnav for fissures and bronchus depiction. Both sequences had similar scores for vessel depiction. Depiction of vessels was significantly better in UTE3D/ZTE3D vnav compared to SPGR3D (p<0.001) and ZTE4D (p=0.025). Overall, fissure depiction was poor on all sequences, with best depiction on ZTE3D vnav (2.06 out of 5.00). The depiction of the bronchi on UTE3D/ZTE3D vnav was significantly better SPGR3D. The noise level was acceptable for UTE3D and ZTE3D vnav, with significantly less noise on UTE3D than all other sequences (p=0.009 for SPGR3D, p=0.003 for ZTE3D vnav, p=0.022 for ZTE3D BH and p=0.041 for ZTE4D). The scores can be seen in Table 4, and the visualisation of them in the Electronic Supplementary Material Fig. S2.

Intra- and interobserver agreement can be seen in Table 5, where good agreement between readers was considered if $\kappa_{inter} \geq 0.6$. Moderate to good agreement was found for most sequences, except for SPGR3D. In addition,

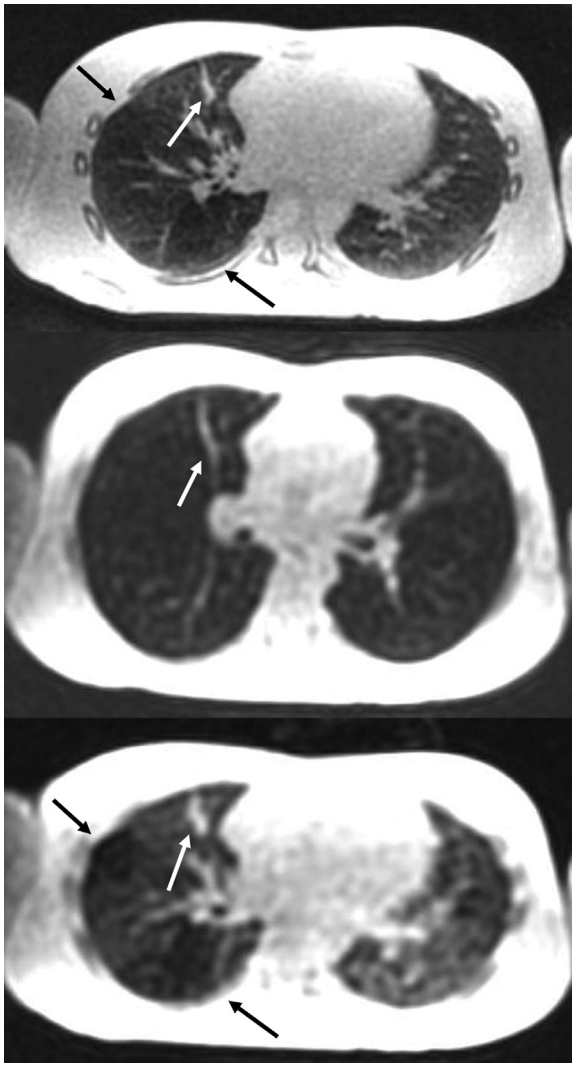

Figure 2 An 8-year-old female patient with severe BPD: (a) 1.5 mm ZTE free-breathing, (b) 3 mm end-inspiratory, and (c) end-expiratory breath-hold SPGR sequences. Note the linear fibrotic rest abnormality in the ventral subpleural part of the right upper lobe, which is better seen on the ZTE image (white arrow in (a)) compared to the SPGR sequences (white arrows in (b) and (c)).

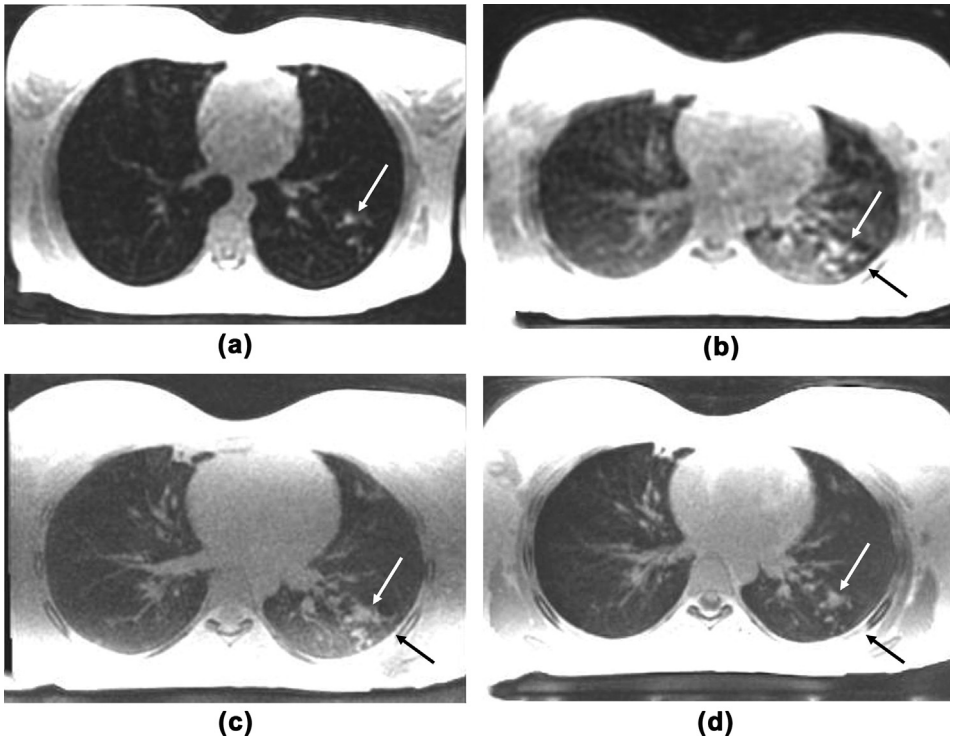

Figure 3 An 18-year-old woman with CF: (a) 3 mm end-inspiratory and (b) end-expiratory breath-hold SPGR, (c) 1.5 mm ZTE (vnav) free breathing with navigated echo triggering, and (d) 1.5 mm UTE free-breathing with pneumo-belt respiratory triggering. Note area of mucus plugging in the left lower lobe, which is better seen in the ZTE and UTE images (white arrow in (c) and (d)) compared to SPGR scans (white arrows in (a) and (b)). Conversely associated air trapping, seen as hypointense lung tissue, is better seen in the expiratory scan breath-hold (black arrow in (b)) being at residual volume and not at residual functional capacity as in ZTE and UTE0 (black arrow in (c) and (d)).

very low agreement was found for the scoring of the fissures on all sequences. The best interobserver agreement was found for UTE3D, while the lowest was found for the detection of lung fissures on all sequences.

Discussion

In the present study, different short and UTE sequences were compared in paediatric patients and healthy volunteers during free breathing and breath-hold conditions to determine the most suitable clinical setting for future paediatric lung MRI examinations.

UTE3D showed the highest overall acceptability from both observers; this may be because of the more consistent gating interface using prospective gating with a pneumo-belt as compared to the other gated sequences and the shorter acquisition time. Image quality of UTE3D was also affected by triggering efficiency and irregular respiratory patterns but may have been more consistent in the patient sample. Pneumo-belts can be more efficient than using the diaphragmatic pen-beam based navigated setup, if the thorax fitting of the pneumo-belt is verified during the examination. On the other hand, in small children, the flexible corrugated tube used for the pneumo-belt did not

Table 3
Comparison of SNR of the lung parenchyma and CNR of the lung parenchyma-blood (LB), lung parenchyma and muscle (LM) and blood muscle (BM) between sequences (mean ± standard deviation).

	Inspiration		Expiration				
	SPGR3D inspiration	ZTE3D BH inspiration	SPGR3D expiration	ZTE3D BH expiration	ZTE3D vnav	UTE3D	ZTE4D
SNR_{out}	8.66 ± 2.49	9.74 ± 3.48	17.74 ± 8.26	12.74 ± 4.17	14.06 ± 4.41	8.23 ± 3.79	15.51 ± 5.38
$SNR_{trachea}$		11.77 ± 2.20		10.64 ± 3.32	13.18 ± 5.50	9.26 ± 3.29	13.80 ± 5.05
CNR_{LB}	17.91 ± 6.80	8.46 ± 3.18	16.39 ± 5.31	9.11 ± 2.58	15.86 ± 5.87	12.56 ± 5.59	10.22 ± 3.95
CNR_{LM}	40.25 ± 19.64	33.09 ± 12.42	27.58 ± 11.13	26.71 ± 10.31	29.92 ± 13.42	20.79 ± 9.55	28.80 ± 17.80
CNR_{BM}	22.03 ± 16.33	23.80 ± 10.68	12.76 ± 9.83	18.43 ± 9.22	14.06 ± 10.73	8.14 ± 5.88	18.59 ± 15.25

The ZTE4D expiratory phase was compared to the expiratory gated UTE3D and ZTE3D vnav. Only volunteers were scanned with all sequences.
SPGR3D BH, breath-hold three-dimensional spoiled gradient; UTE3D, three-dimensional ultra-short echo time; ZTE3D vnav, three-dimensional prospective projection navigated radial zero echo time; ZTE4D, four-dimensional zero echo time; ZTE3D BH, breath-hold three-dimensional zero echo time; SNR_{out}, signal-to-noise ratio outside the chest; $SNR_{trachea}$, signal-to-noise ratio in the trachea inner lumen CNR, contrast to noise ratio: CNR_{LB}, CNR lung–blood; CNR_{LM}, CNR lung–muscle; CNR_{BM}, CNR blood–muscle.

Table 4
Qualitative assessment of all sequences in expiratory phase.

	SPGR3D	UTE3D	ZTE3D vnav	ZTE4D	ZTE3D BH
Vessels	2.21 ±0.66	3.24 ±0.77	3.24 ± 0.56	2.36 ± 0.63	2.22 ± 0.67
Fissures	1.25 ± 0.34	2.05 ±0.49	2.06 ± 0.25	1.60 ± 0.63	1.22 ± 0.44
Bronchus	1.88 ± 0.45	3.47 ± 0.87	3.56 ± 0.63	2.27 ± 0.70	2.33 ± 0.86
Noise/ artefacts	2.67 ± 0.70	3.52 ± 1.03	3.0 ± 0.61	2.36 ± 0.74	2.44 ± 0.53
Acceptability	2.33 ± 0.64	3.81 ± 0.98	3.71 ± 0.69	2.79 ± 0.58	2.44 ± 0.53

Data are presented as mean ± standard deviation. Only volunteers were scanned with all sequences.
SPGR3D BH, breath-hold three-dimensional spoiled gradient; UTE3D, three-dimensional ultra-short echo time; ZTE3D vnav, three-dimensional prospective projection navigated radial zero echo time; ZTE4D, four-dimensional zero echo time; ZTE3D BH, breath-hold three-dimensional zero echo time.

provide appropriate respiratory recording each time and it had to be adjusted during acquisition.[5] Unfortunately, the gain on the respiratory signal recorded could not be modified as it was automatically adjusted by the patient monitoring unit dependent on the maximum excursion of the signal recorded from the pneumo-belt. The ZTE3D vnav sequence was silent and feedback from the gradient noise was not possible for the patient, therefore the triggering threshold tended to drift and had to be constantly adjusted so that trigger efficiency could be maintained. Regarding SNR and CNR, UTE3D did not show the highest scores.

The larger voxel size and the deeper expiratory level (higher water content in the acquired voxel) can explain the higher SNR of breath-hold expiratory SPGR3D compared to UTE3D and ZTE3D vnav scans despite the longer TE of the former (TE of 0.6 ms instead of around 0 ms).

ZTE3D vnav provided good image quality for the bronchi, giving high-resolution structural information with better depiction of intrapulmonary structures than the other sequences. Better depiction of bronchi with ZTE3D vnav was attained by overall higher SNR than UTE3D with the same spatial resolution. ZTE3D vnav had 12.5% of the voxel size compared to SPGR3D, while voxel size for ZTE3D BH was around 60%. This voxel size is still larger than the standard CT voxel size, which is usually 1 mm isotropic.[32,33]

ZTE3D BH offered similar advantages to the navigated version providing enhanced signal of the lung parenchyma during breath-holding, and therefore, more efficient scanning and less artefacts overall. A major limitation of the choice of parameters for ZTE3D BH was the long scan time to achieve good SNR. The 20 second breath-hold scan duration was not feasible in small children, who usually cannot hold their breath longer than 10 seconds. The scan duration of ZTE3D BH could not be reduced to $<$10 seconds, because the SNR would have not been adequate. The voxel resolution was set between the voxel resolution of the breath-hold SPGR3D and the higher voxel resolution of the respiratory gated counterparts (ZTE3D vnav and UTE3D) acquisitions yet taking into consideration the SNR that could be obtained. ZTE4D was acquired at the same resolution as the ZTE3D BH scan. The idea behind comparing ZTE3D BH to ZTE4D at different inspiratory levels was to have a good reference for blurring and artefacts that the implementation of ZTE4D showed during most of the reconstructed phases. During sequence tuning, the number of spokes per segment was varied to investigate if better fidelity could be achieved with ZTE4D, but this was not the case.

As an alternative to ZTE3D BH, we also tested ZTE4D, with the idea to capture both inspiratory and expiratory phases in a single free-breathing acquisition. Throughout the acquisition the respiratory rate and excursion of the breathing pattern have to be constant to provide consistent results with the current implementation of ZTE4D. Unfortunately, the results from the healthy volunteers were not positive. Despite the apparent constant respiratory pattern observed in the recorded pneumo-belt signal, ZTE4D

Table 5
Intra- and inter correlation coefficients for all the sequences. Data are presented as intra correlation coefficient (ICC).

	SPGR3D insp.	SPGR3D Exp.	UTE3D	ZTE3D vnav	ZTE4D	ZTE3D BH
Intra CC values						
Vessels	0.302	0.291	0.684	0.529	0.533	0.391
Fissures	0.286	0.156	0.231	0.091	0.345	0.273
Bronchus	0.114	0.243	0.624	0.607	0.675	0.600
Noise/artefacts	0.650	0.721	0.859	0.586	0.395	0.111
Acceptability	0.269	0.284	0.910	0.463	0.717	0.429
Inter CC values						
Vessels	0.230	0.659	0.837	0.566	0.128	0.333
Fissures	0.150	0.156	0.674	0.119	0.276	0.500
Bronchus	0.491	0.419	0.756	0.655	0.368	0.562
Noise/artefacts	0.791	0.639	0.762	0.264	0.551	0.444
Acceptability	0.497	0.455	0.740	0.552	0.513	0.250

Four patients and all volunteers were scanned with all sequences.
SPGR3D BH, breath-hold three-dimensional spoiled gradient; UTE3D, three-dimensional ultra-short echo time; ZTE3D vnav, three-dimensional prospective projection navigated radial zero echo time; ZTE4D, four-dimensional zero echo time; ZTE3D BH, breath-hold three-dimensional zero echo time.

showed considerable ghosting/blurring/streaking artefacts in most of the reconstructed phases.

Due to the appearance of artefacts from the coils in the background outside of the chest for both ZTE3D and UTE3D sequences, the SNR calculation was performed with two different background noise ROIs. One was taken from an area of the background outside the chest where artefacts could be avoided and the other was taken from the trachea lumen. This double approach on SNR measurements was influenced by the choice of FOV size of the ZTE sequences. For ZTE sequences, the scan duration depends on the FOV. To keep scan durations as short as possible at the desired resolution, the FOV was smaller, therefore ROIs taken from the background could have included artefactual signal and noise coming from the coil elements and coil casings. It is unclear how to deal with the right standard deviation of the noise inside the trachea because of possible artefacts. The mean background intensity measured in the trachea in both UTE3D and ZTE3D scans was always lower than air regions outside the chest cavity.

MRI settings for ZTE3D and UTE3D did not differ significantly in terms of spatial resolution and acquisition time from those of previous studies, including that of Bae *et al.*[29] The present study used an isotropic voxel size of 1.5 mm versus 1.4 mm used by Bae at al.[35] Nonetheless, the major difference was that both studies of Bae *et al.* (2019, 2020) were performed using 3 T. A second major difference between Bae *et al.* (2020) and the present settings was that ZTE3D/ZTE4D was acquired at the higher readout bandwidth of 62.5 kHz compared to 31.5 kHz. The present protocol required more averaging/number of spokes per segment to compensate for the lower SNR at the lower field strength and the higher readout bandwidths used. It was assumed that the degree of blurring in the present scans due to shorter T2* species would be less with the present settings.

Finally, the qualitative measurements showed moderate to good intra- and interobserver variability for most sequences, except for SPGR3D in- and end-expiration. The most difficult structures to assess were lung fissures, which were very poorly identified on all MRI sequences by both readers.

The present study has some limitations. Firstly, not all sequences were performed in the paediatric cohort, mainly because of the scanning duration for each study. For each sequence, the best spatial resolution achievable with the desired/allowed scan duration per patient/volunteer was chosen to provide better visualisation of the target abnormality within the patient population. This did not allow direct comparison of the diagnostic value of each technique. Moreover, each sequence was used with different purposes also taking into account different respiratory levels. The expiratory breath-hold SPGR3D sequence was used to assess trapped air and the ZTE3D and UTE3D sequences were used to look for airway pathologies (i.e., bronchiectasis) and parenchymal abnormalities (i.e., consolidation, mucus plugs). Secondly, no attempt was made to try to match the scan duration of UTE3D and ZTE3D vnav to provide a fairer comparison. The readout bandwidths for both UTE3D and ZTE3D readouts was set to a similar value (62.5 kHz). Nonetheless, the ZTE readout is more time efficient than that of a UTE readout (around 1 ms for ZTE versus 5 ms for UTE). The readout period during the expiratory period was typically shorter for ZTE3D vnav than for UTE3D. To maintain a shorter acquisition time for UTE3D, the readout time was slightly elongated (reflecting the time difference between acquisitions as shown on the table). The UTE3D sequence has also a slightly different readout strategy; it uses a partially twisted k-space trajectory (CONES) that can cover a larger portion of k-space (raw data space) in comparison to the pure radial readout of ZTE3D/ZTE4D (see Table 1). It was therefore decided to make some compromises during sequence settings in order to match the set voxel resolution with a reasonable scan duration for patients. An attempt was made to limit the scan duration between 5 to 10 minutes per sequence, depending on respiratory triggering and respiratory frequency. Longer scan durations would not be feasible in a clinical setting, regarding patient compliance and for the maximum total scan duration allowed (no longer than 45 minutes per study).

In conclusion, the aim of the present study was to test the feasibility and image quality of different short and UTE sequences for paediatric lung MRI. Based on the results, ZTE3D vnav provides the most reliable output in terms of image quality, although it can be affected by triggering efficiency and irregular respiratory patterns. UTE3D also provides high image quality, but pneumo-belt respiratory triggering is currently inadequate in small children, where the fitting of the pneumo-belt is poor. The current implementation of ZTE4D does not provide diagnostic image quality for all acquisition phases. Future implementation of respiratory-gated ZTE3D and UTE3D should focus on improvements of respiratory triggering with a pneumo-belt that is more amenable for small patients or on providing better diaphragmatic navigator options.

Declaration of competing interests

The authors declare the following financial interests/personal relationships which may be considered as potential competing interests: Mika Vogel - GE Healthcare employee, Pierluigi Ciet – GE Healthcare research collaboration.

Appendix A. Supplementary data

Supplementary data to this article can be found online at https://doi.org/10.1016/j.crad.2022.12.020.

References

1. Zucker EJ, Cheng JY, Haldipur A, *et al.* Free-breathing paediatric chest MRI: performance of self-navigated golden-angle ordered conical ultrashort echo time acquisition. *J Magn Reson Imaging* 2018;**47**:200–9. https://doi.org/10.1002/jmri.25776.
2. Macdougall RD, Strauss KJ, Lee EY. Managing radiation dose from thoracic multidetector computed tomography in paediatric patients: background, current issues, and recommendations. *Radiol Clin North Am* 2013;**51**:743–60.

3. Pearce MS, Salotti JA, Little MP, *et al*. Radiation exposure from CT scans in childhood and subsequent risk of leukaemia and brain tumours: a retrospective cohort study. *Lancet* 2012;**380**:499–505.
4. Tiddens HA, Stick SM, Wild JM, *et al*. Respiratory tract exacerbations revisited: ventilation, inflammation, perfusion, and structure (VIPS) monitoring to redefine treatment. *Paediatr Pulmonol* 2015;**50**(Suppl. 40):S57–65. https://doi.org/10.1002/ppul.23266.
5. Ciet P, Tiddens HA, Wielopolski PA, *et al*. Magnetic resonance imaging in children: common problems and possible solutions for lung and airways imaging. *Paediatr Radiol* 2015;**45**(13):1901–15. https://doi.org/10.1007/s00247-015-3420-y.
6. Bergin CJ, Glover GH, Pauly JM. Lung parenchyma: magnetic susceptibility in MR imaging. *Radiology* 1991;**180**:845–8. https://doi.org/10.1148/radiology.180.3.1871305.
7. Wild JM, Marshall H, Bock M, *et al*. MRI of the lung (1/3): methods. *Insights Imaging* 2012;**3**:345–53. https://doi.org/10.1007/s13244-012-0176-x.
8. Bergin CJ, Pauly JM, Macovski A. Lung parenchyma: projection reconstruction MR imaging. *Radiology* 1991;**179**:777–81. https://doi.org/10.1148/radiology.179.3.2027991.
9. Biederer J, Mirsadraee S, Beer M, *et al*. MRI of the lung (3/3)-current applications and future perspectives. *Insights Imaging* 2012;**3**:373–86. https://doi.org/10.1007/s13244-011-0142-z.
10. Biederer J, Hintze C, Fabel M. MRI of pulmonary nodules: technique and diagnostic value. *Cancer Imaging* 2008;**8**:125–30. https://doi.org/10.1102/1470-7330.2008.0018.
11. Iwasawa T, Takahashi H, Ogura T, *et al*. Correlation of lung parenchymal MR signal intensity with pulmonary function tests and quantitative computed tomography (CT) evaluation: a pilot study. *J Magn Reson Imaging* 2007;**26**:1530–6. https://doi.org/10.1002/jmri.21183.
12. Bankier AA, O'Donnell CR, Mai VM, *et al*. Impact of lung volume on MR signal intensity changes of the lung parenchyma. *J Magn Reson Imaging* 2004;**20**(6):961–6. https://doi.org/10.1002/jmri.20198.
13. Bauman G, Puderbach M, Deimling M, *et al*. Non-contrast-enhanced perfusion and ventilation assessment of the human lung by means of Fourier decomposition in proton MRI. *Magn Reson Med* 2009;**62**:656–64. https://doi.org/10.1002/mrm.22031.
14. Ley-Zaporozhan J, Ley S, Eberhardt R, *et al*. Visualization of morphological parenchymal changes in emphysema: comparison of different MRI sequences to 3D-HRCT. *Eur J Radiol* 2010;**73**:43–9. https://doi.org/10.1016/j.ejrad.2008.09.029.
15. Puderbach M, Hintze C, Ley S, *et al*. MR imaging of the chest: a practical approach at 1.5 T. *Eur J Radiol* 2007;**64**(3):345–55. https://doi.org/10.1016/j.ejrad.2007.08.009.
16. Peltola V, Ruuskanen O, Svedström E. Magnetic resonance imaging of lung infections in children. *Paediatr Radiol* 2008;**38**:1225–31. https://doi.org/10.1007/s00247-008-0987-6.
17. Ley-Zaporozhan J, Ley S, Sommerburg O, *et al*. Clinical application of MRI in children for the assessment of pulmonary diseases. *Rofo* 2009;**181**:419–32. https://doi.org/10.1055/s-0028-1109128.
18. Failo R, Wielopolski PA, Tiddens HA, *et al*. Lung morphology assessment using MRI: a robust ultra-short TR/TE 2D steady state free precession sequence used in cystic fibrosis patients. *Magn Reson Med* 2009;**61**:299–306. https://doi.org/10.1002/mrm.21841.
19. Wagner M, Böwing B, Kuth R, *et al*. Low field thoracic MRI—a fast and radiation free routine imaging modality in children. *Magn Reson Imaging* 2001;**19**:975–83. https://doi.org/10.1016/s0730-725x(01)00417-9.
20. Rupprecht T, Kuth R, Bowing B, *et al*. Sedation and monitoring of paediatric patients undergoing open low-field MRI. *Acta Paediatr* 2000;**89**:1077–81.
21. Serra G, Milito C, Mitrevski M, *et al*. Lung MRI as a possible alternative to CT scan for patients with primary immune deficiencies and increased radiosensitivity. *Chest* 2011;**140**:1581–9. https://doi.org/10.1378/chest.10-3147.
22. Stern M, Wiedemann B, Wenzlaff P. German cystic fibrosis quality assessment group. From registry to quality management: the German cystic fibrosis quality assessment project 1995 2006. *Eur Respir J* 2008;**31**:29–35. https://doi.org/10.1183/09031936.00056507.
23. Gibson RL, Burns JL, Ramsey BW. Pathophysiology and management of pulmonary infections in cystic fibrosis. *Am J Respir Crit Care Med* 2003;**168**:918–51. https://doi.org/10.1164/rccm.200304-505SO.
24. Puderbach M, Eichinger M, Gahr J, *et al*. Proton MRI appearance of cystic fibrosis: comparison to CT. *Eur Radiol* 2007;**17**:716–24. https://doi.org/10.1007/s00330-006-0373-4.
25. Puderbach M, Eichinger M, Haeselbarth J, *et al*. Assessment of morphological MRI for pulmonary changes in cystic fibrosis (CF) patients: comparison to thin-section CT and chest x-ray. *Invest Radiol* 2007;**42**:715–25. https://doi.org/10.1097/RLI.0b013e318074fd81.
26. Eichinger M, Puderbach M, Fink C, *et al*. Contrast-enhanced 3D MRI of lung perfusion in children with cystic fibrosis—initial results. *Eur Radiol* 2006;**16**(10):2147–52. https://doi.org/10.1007/s00330-006-0257-7.
27. Biederer J, Beer M, Hirsch W, *et al*. MRI of the lung (2/3). Why...-when...how? *Insights Imaging* 2012;**3**:355–71. https://doi.org/10.1007/s13244-011-0146-8.
28. Gibiino F, Sacolick L, Menini A, *et al*. Free-breathing, zero-TE MR lung imaging. *MAGMA* 2015;**28**:207–15. https://doi.org/10.1007/s10334-014-0459-y.
29. Bae K, Jeon KN, Hwang MJ, *et al*. Comparison of lung imaging using three-dimensional ultrashort echo time and zero echo time sequences: preliminary study. *Eur Radiol* 2019;**29**:2253–62. https://doi.org/10.1007/s00330-018-5889-x.
30. Dournes G, Menut F, Macey J, *et al*. Lung morphology assessment of cystic fibrosis using MRI with ultra-short echo time at submillimeter spatial resolution. *Eur Radiol* 2016;**26**:3811–20. https://doi.org/10.1007/s00330-016-4218-5.
31. Renz DM, Herrmann KH, Kraemer M, *et al*. Ultrashort echo time MRI of the lung in children and adolescents: comparison with non-enhanced computed tomography and standard post-contrast T1w MRI sequences. *Eur Radiol* 2022;**32**:1833–42. https://doi.org/10.1007/s00330-021-08236-7.
32. Niwa T, Nozawa K, Aida N. Visualization of the airway in infants with MRI using pointwise encoding time reduction with radial acquisition (PETRA). *J Magn Reson Imaging* 2017;**45**:839–44. https://doi.org/10.1002/jmri.25420.
33. Yu J, Xue Y, Song HK. Comparison of lung T2* during free-breathing at 1.5 T and 3.0 T with ultrashort echo time imaging. *Magn Reson Med* 2011;**66**:248–54. https://doi.org/10.1002/mrm.22829.
34. Hatabu H, Alsop DC, Listerud J, *et al*. T2* and proton density measurement of normal human lung parenchyma using submillisecond echo time gradient echo magnetic resonance imaging. *Eur J Radiol* 1999;**29**:245–52. https://doi.org/10.1016/s0720-048x(98)00169-7.
35. Bae K, Jeon KN, Hwang MJ, *et al*. Respiratory motion-resolved four-dimensional zero echo time (4D ZTE) lung MRI using retrospective soft gating: feasibility and image quality compared with 3D ZTE. *Eur Radiol* 2020;**30**:5130–8. https://doi.org/10.1007/s00330-020-06890-x.